Electronic Supplementary Material (ESI) for Energy & Environmental Science.

Electronic Supplementary Information

Towards Watt-scale hydroelectric energy harvesting by $Ti_3C_2T_x$-based transpiration-driven electrokinetic power generators

Jaehyeong Bae[a,b,†], Min Soo Kim[b,†], Taegon Oh[c], Bong Lim Suh[d], TaeGwang Yun[e], Seungjun Lee[c,f], Kahyun Hur[d], Yury Gogotsi[g], Chong Min Koo[c,f,h] & Il-Doo Kim[b,*]

[a]John A. Paulson School of Engineering and Applied Science, Harvard University, Cambridge, MA 02138, USA

[b]Department of Materials Science and Engineering, Korea Advanced Institute of Science and Technology (KAIST), 291 Daehak-ro, Yuseong-gu, Daejeon, 34141, Republic of Korea.

[c]Materials Architecturing Research Center, Korea Institute of Science and Technology, Seoul 02792, Republic of Korea.

[d]Extreme Materials Research Center, Advanced Materials Research Division, Korea Institute of Science and Technology, Seoul 02792, Republic of Korea.

[e]Department of Materials Science and Engineering, Myongji University, Yongin, Gyeonggi 17058, Republic of Korea.

[f]KU-KIST Graduate School of Converging Science and Technology, Korea University, Seoul 02841, Korea.

[g]Department of Materials Science and Engineering, and A. J. Drexel Nanomaterials Institute, Drexel University, 3141 Chestnut Street, Philadelphia, PA 19104, USA.

[h]Division of Nano & Information Technology, KIST School, University of Science and Technology, Seoul 02792, Republic of Korea.

†These authors contributed equally to this work.

*Correspondence to: Il-Doo Kim; idkim@kaist.ac.kr

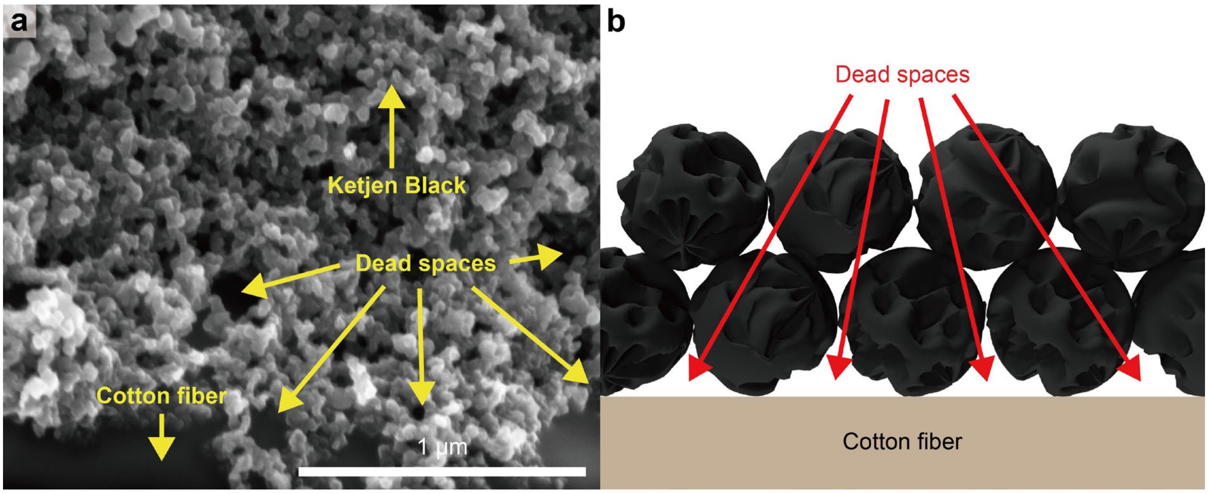

Fig. S1 Geometrical disadvantage of carbon nanoparticles (Ketjen black) for the transpiration driven electrokinetic power generator (TEPG). (a) Scanning electron microscope image of Ketjen black coated cotton membrane. Plenty of dead spaces locates between cotton membrane and Ketjen blacks, and between Ketjen black particles. **(b)** Schematic illustration of carbon nanoparticles coated cotton membrane. The dead space originates from morphology of carbon nanoparticles.

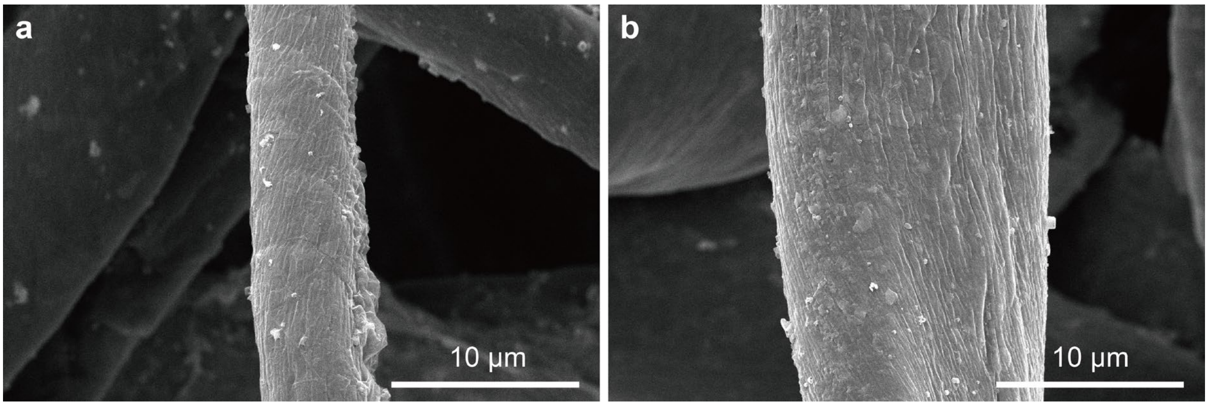

Fig. S2 Structural integrity of $Ti_3C_2T_x$ coating on cotton fiber. SEM images of **(a)** $Ti_3C_2T_x$-coated cotton fiber before operation and **(b)** $Ti_3C_2T_x$-coated cotton fiber after 10 cycles of operation.

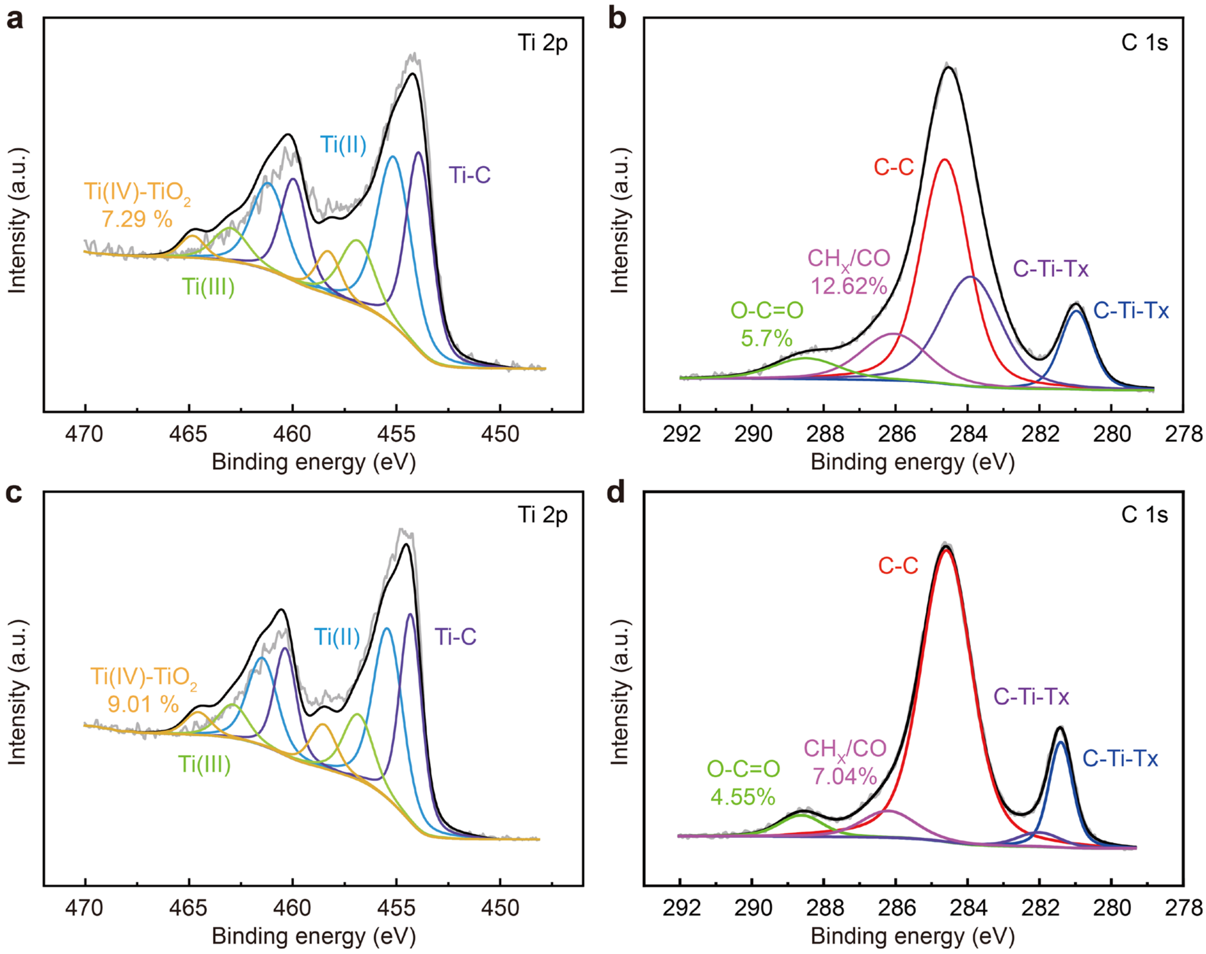

Fig. S3 X-ray photoelectron spectroscopy (XPS) spectra of $Ti_3C_2T_x$ on MXene ($Ti_3C_2T_x$)-based TEPG (MTEPG) before and after operation. (a) Ti 2p peak from pristine MTEPG. **(b)** C 1s peak from pristine MTEPG. **(c)** Ti 2p peak from MTEPG after an operation by 30 μL of water. **(d)** C 1s peak from MTEPG after an operation by 30 μL of water. Chemical states and binding energies of deconvoluted peaks are listed in Table S3[1]. The oxidation-related Ti(IV)-TiO_2 peak intensity increased from 7.29% to 9.01% after operation. However, such oxidation is negligible compared to the reported oxidation rate of $Ti_3C_2T_x$ in wet air[2].

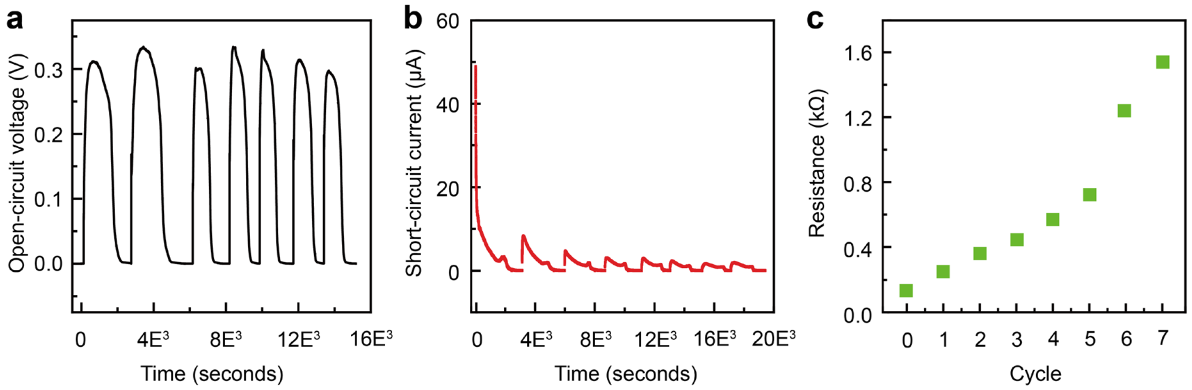

Fig. S4 Performance variation of $Ti_3C_2T_x$-based TEPG (MTEPG) over multiple cycles. Performance of a 130 Ω MTEPG device in multiple operation cycles is shown in **(a).** The periodicity of V_{OC} output varies due to the daily temperature and humidity differences. The first two peaks were generated under high humidity condition (22 °C, RH ~ 65%), and the other cycles were done under lower humidity conditions (24 °C, RH ~ 50%). **(b)** short-circuit current and **(c)** resistance.

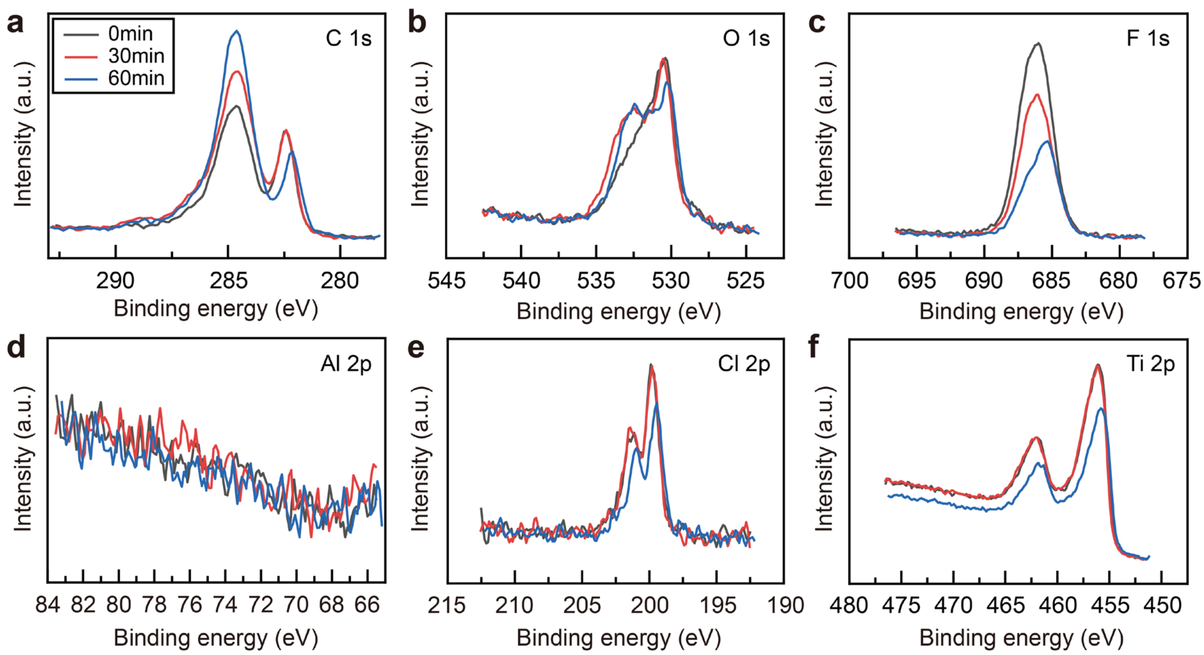

Fig. S5 XPS data of pristine, 30-min sonicated, 60-min sonicated $Ti_3C_2T_x$ MXene. (a)-(f), C 1s, O 1s, F 1s, Al 2p, Cl 2p, and Ti 2p peak from pristine and sonicated $Ti_3C_2T_x$ MXene.

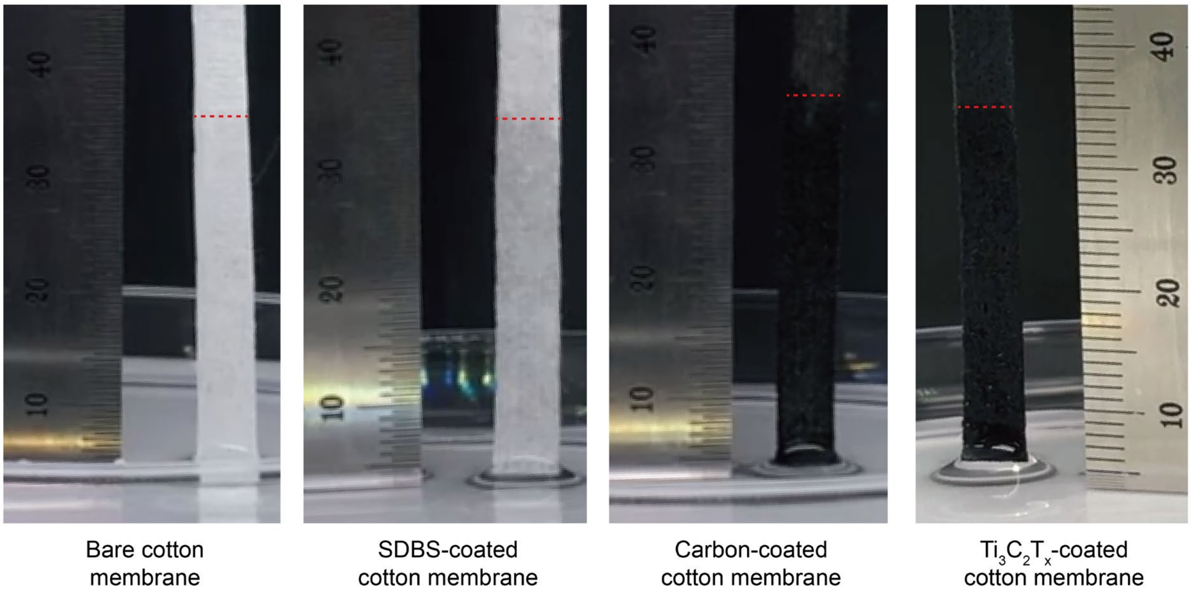

Fig. S6 Vertical wicking rate measurement of the bare cotton membrane, SDBS-coated cotton membrane, carbon-coated cotton membrane, and $Ti_3C_2T_x$-coated cotton membrane. The size of the membranes was 7 cm × 0.5 cm × 0.12 mm. The red dotted line shows the wicking frontier through the membrane. The wicking rate was analyzed by measuring the time to reach 3.5 cm of the membrane.

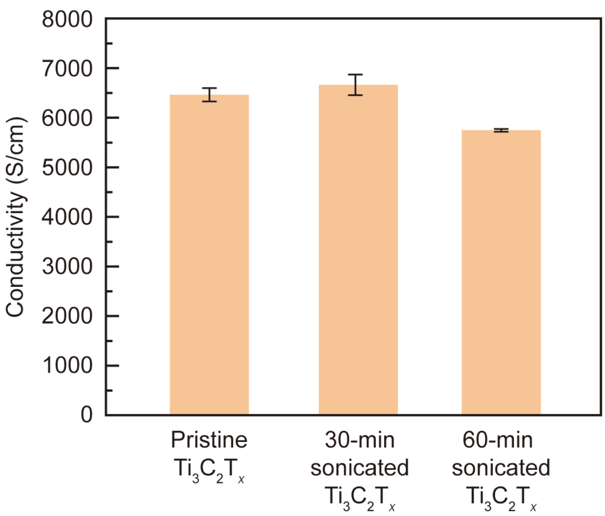

Fig. S7 Electrical conductivity of pristine, 30-min sonicated, 60-min sonicated $Ti_3C_2T_x$ MXene.

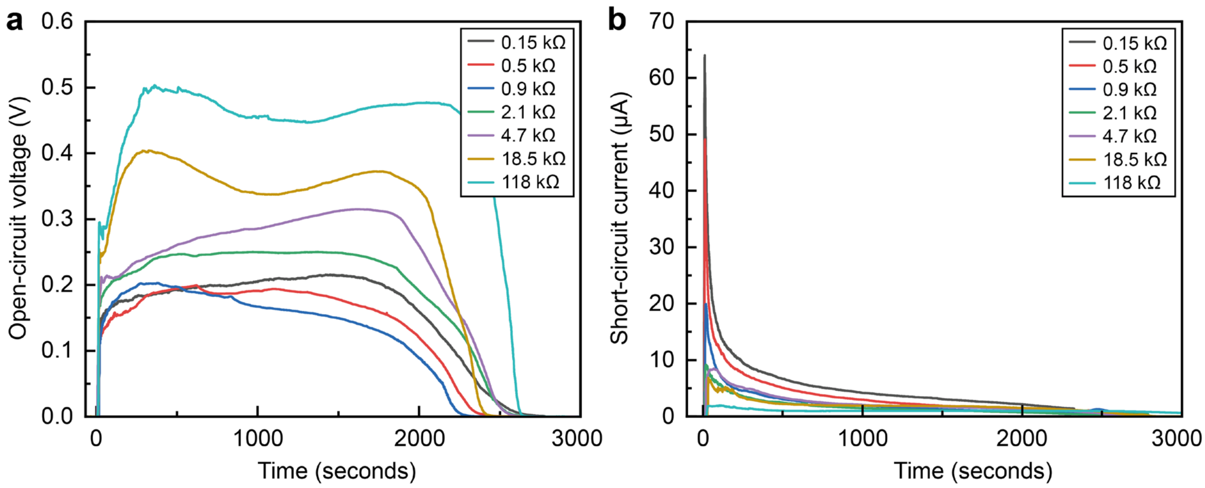

Fig. S8 Measured open-circuit voltage (V_{OC}) and short circuit current (I_{SC}) of MTEPG with varying the bulk resistance by dropping 30 μL of DI water.

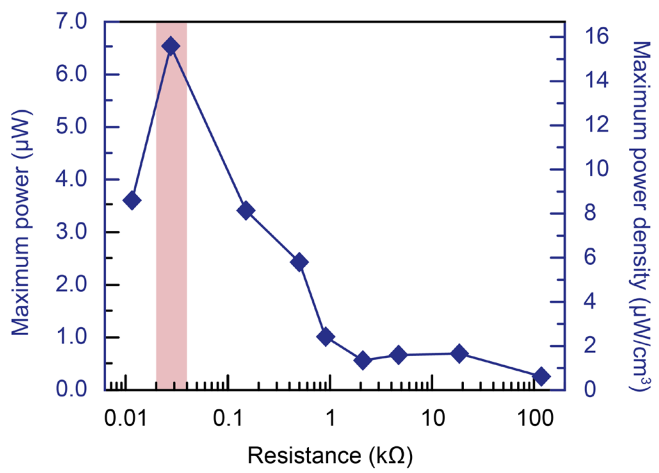

Fig. S9 Generated power and power density from the MTEPG versus bulk resistance.

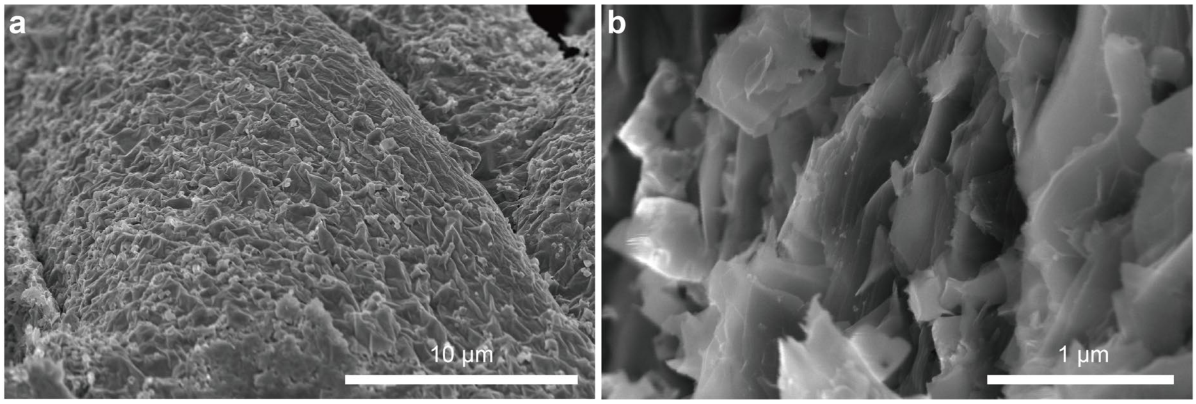

Fig. S10 Reduced degree of orientation $Ti_3C_2T_x$ sheets in MTEPG with low bulk resistance (<15 Ω). (a) SEM and **(b)** enlarged SEM image of MTEPG (<15 Ω).

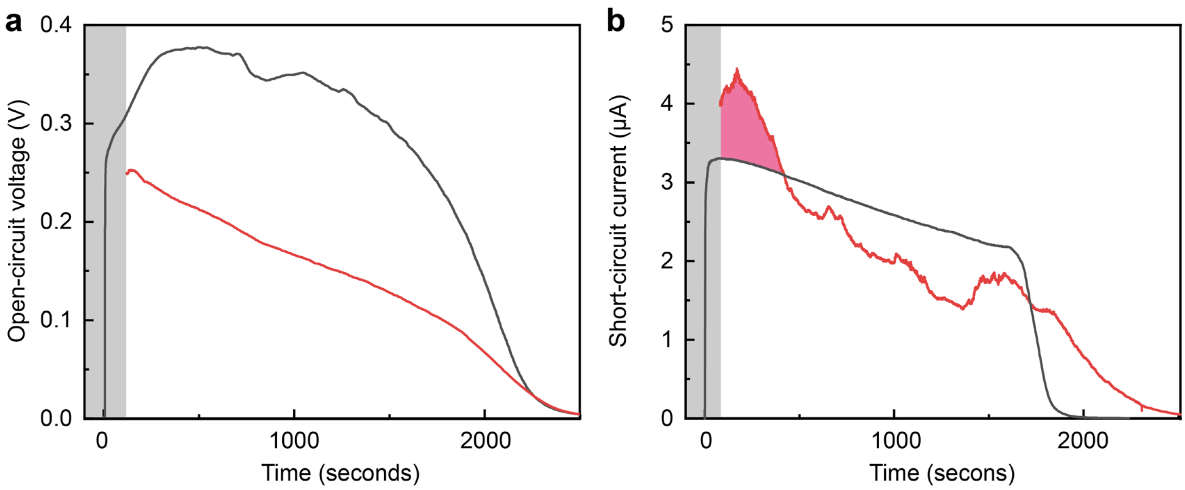

Fig. S11 Measured V_{OC} and I_{SC} profiles of cTEPG starting from water-dropping (gray line) and 2 min after water dropping (red line). The pink region is the charge amount (0.31 mC) accumulated under the open-circuit conditions for the first 2 min. The non-delayed gray region corresponds to the charge of 0.36 mC.

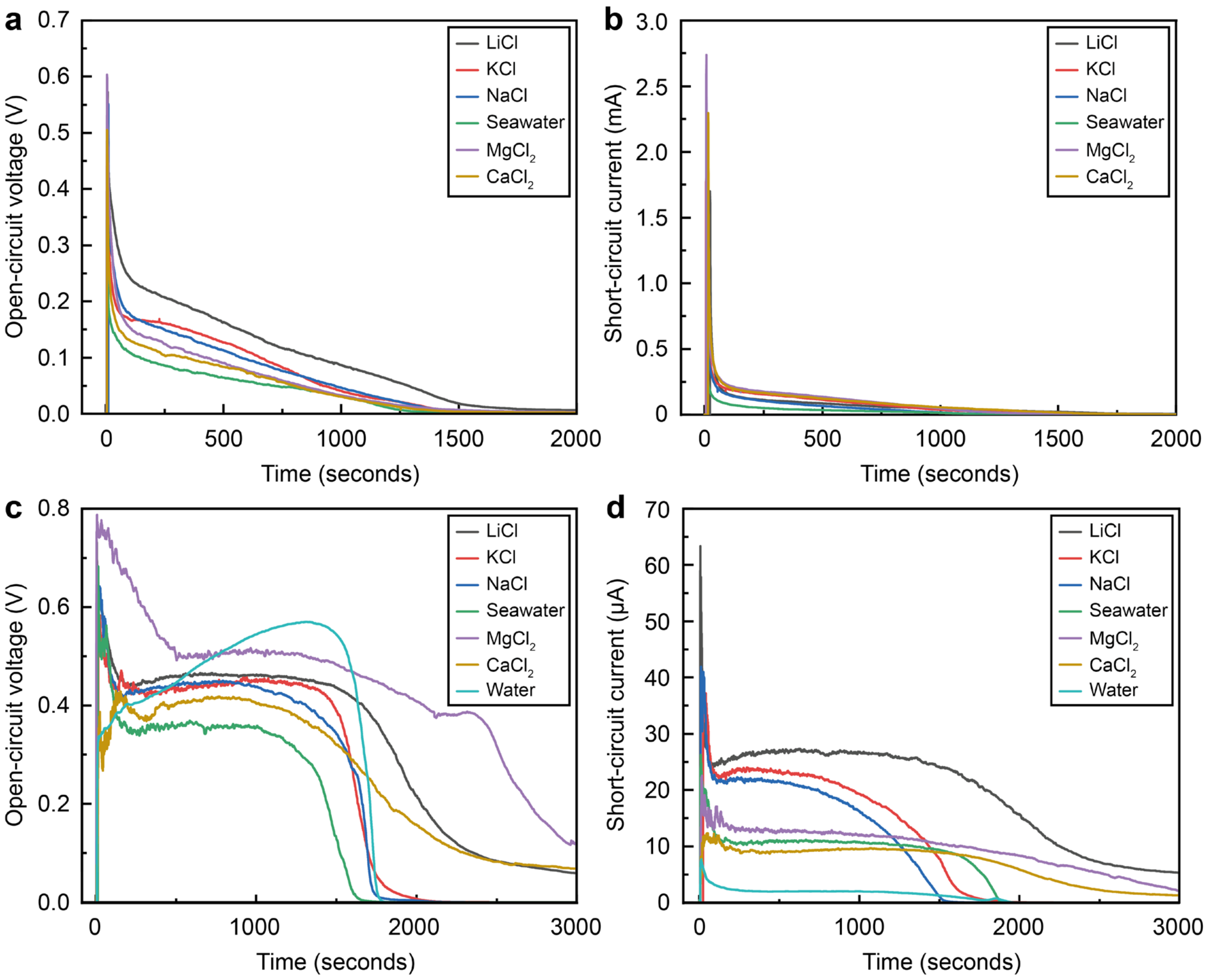

Fig. S12 Measured V_{OC} and I_{SC} from MTEPG of 150 Ω (a, b) and 120 kΩ (c, d) by dropping 30 μL of 1 M of various electrolyte solutions.

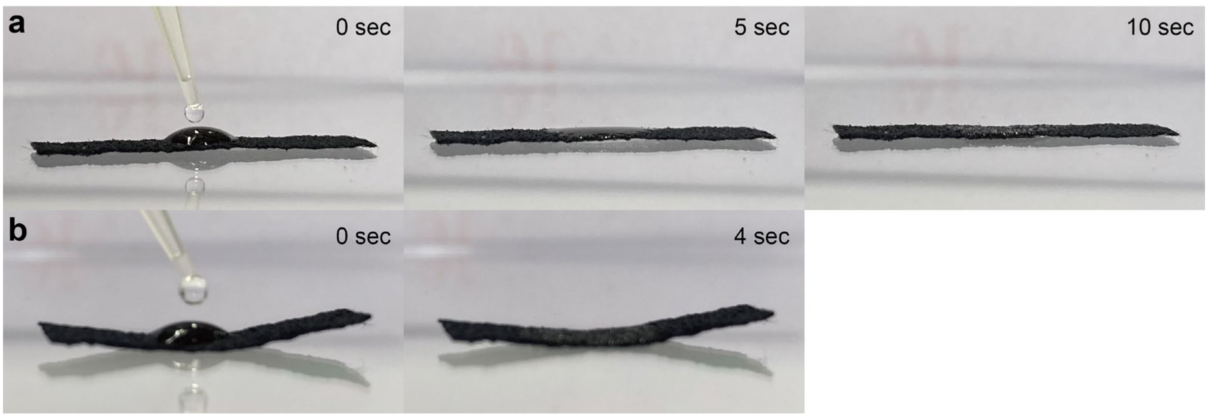

Fig. S13 Photographic images of sluggish adsorption of $CaCl_2$ (a) and $MgCl_2$ (b) solution into MTEPG.

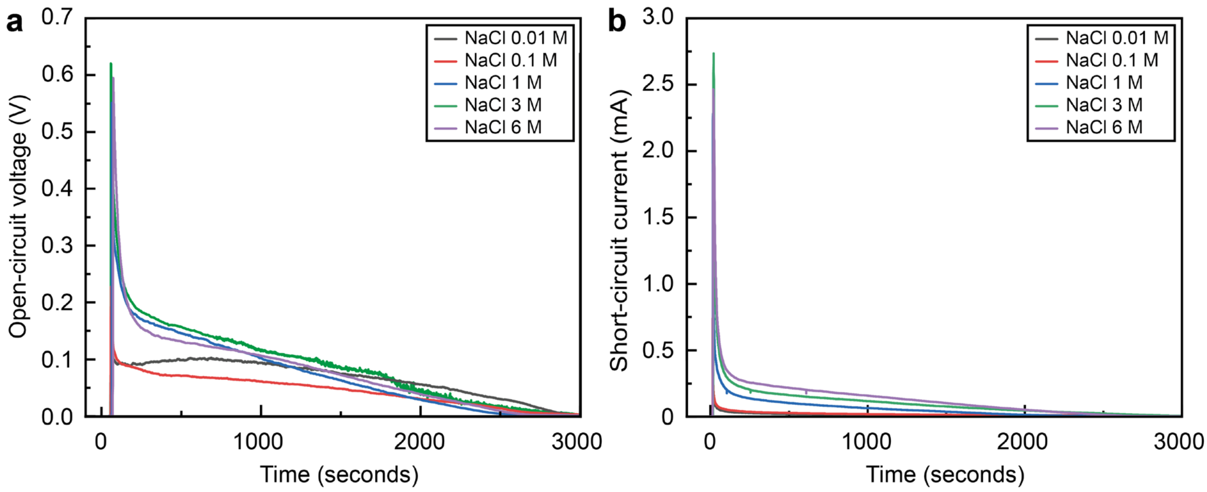

Fig. S14 Measured V_{OC} and I_{SC} from MTEPG (150 Ω) by dropping 30 μL of NaCl solution with various concentrations.

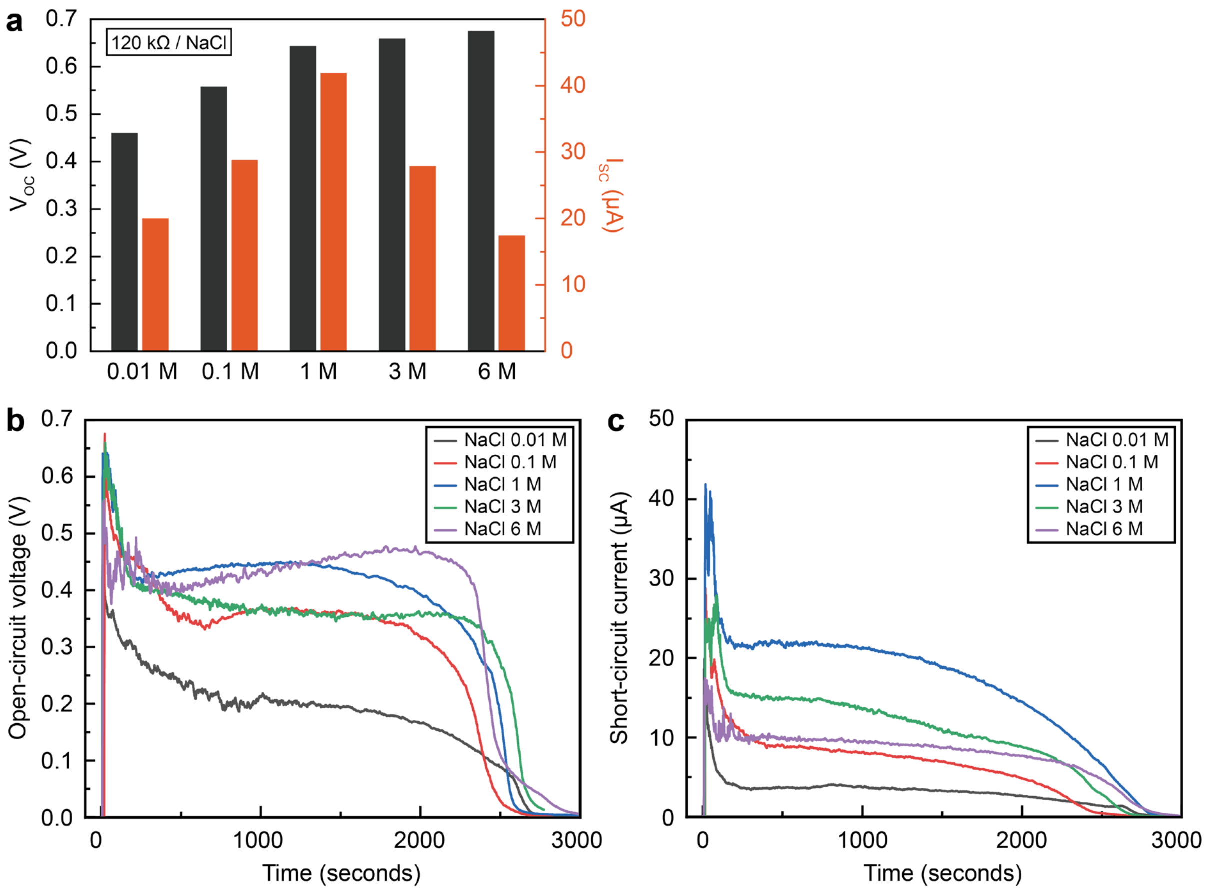

Fig. S15 Measured V_{OC} and I_{SC} from MTEPG (120 kΩ) by dropping 30 μL of NaCl solution with various concentrations.

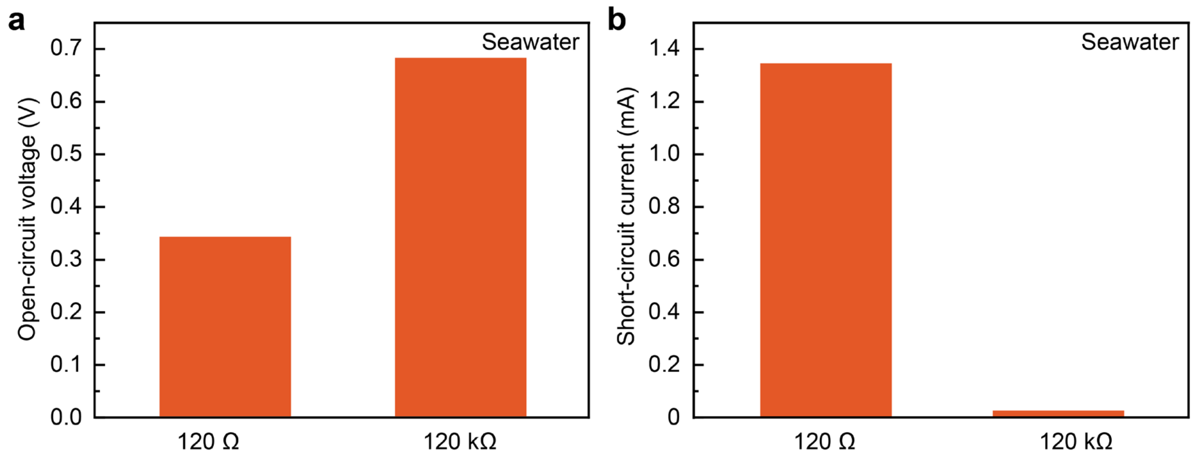

Fig. S16 Measured V_{OC} and I_{SC} from MTEPG (120 Ω and 120 kΩ) by dropping 30 μL of seawater.

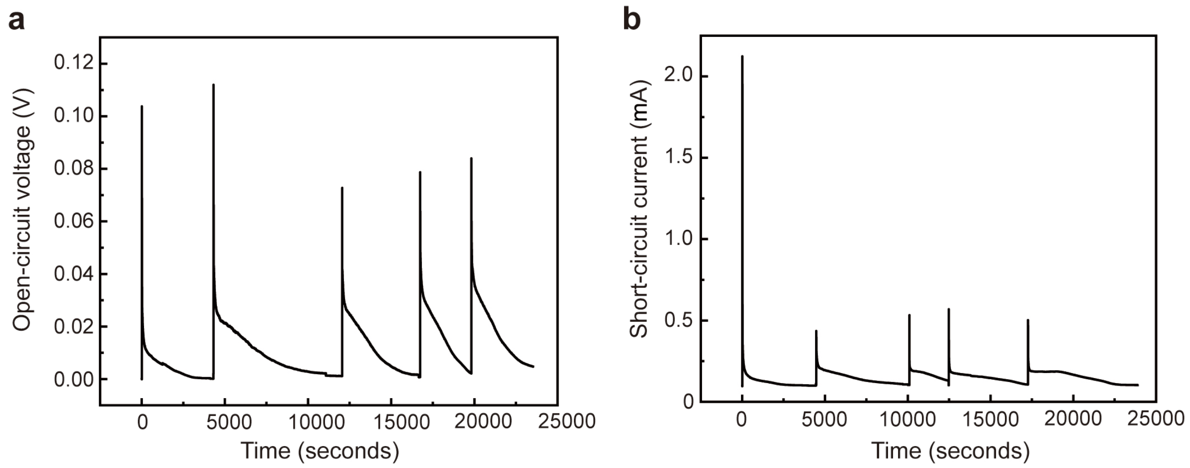

Fig. S17 Measured V_{OC} and I_{SC} of MTEPG (42 Ω) by dropping 30 μL of 1M NaCl solution with various concentrations.

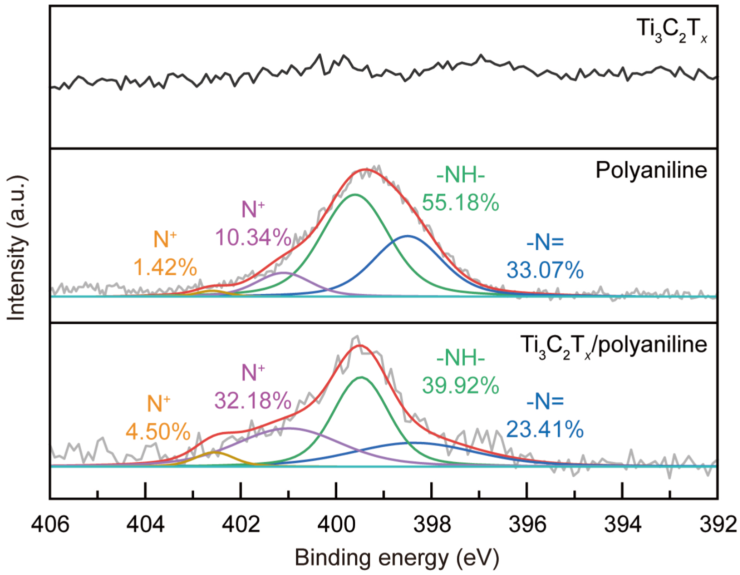

Fig. S18 N 1s XPS data of $Ti_3C_2T_x$, polyaniline emeraldine-base, and $Ti_3C_2T_x$/polyaniline composite. $Ti_3C_2T_x$ has no characteristic N 1s peak. Polyaniline exhibits 4 deconvoluted peaks, corresponding to imine nitrogen (–N=), amine nitrogen (–NH–), and nitrogen radicals (N^+)[3–6]; detailed information of chemical states and binding energies are listed in Table S4. The atomic percentages N^+ peak of polyaniline was increased from 11.76% to 36.68% after mixing with $Ti_3C_2T_x$, proving that polyaniline emeraldine-base (insulating) was transformed into emeraldine-salt (conducting) by $Ti_3C_2T_x$[4].

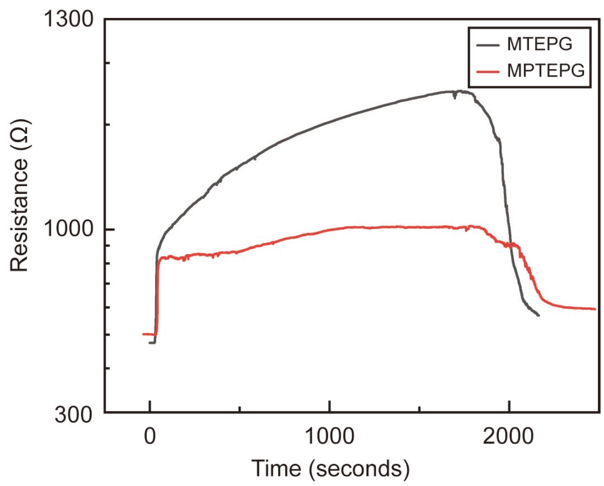

Fig. S19 Bulk resistance change of MTEPG and MXene ($Ti_3C_2T_x$)-polyaniline based TEPG (MPTEPG) during energy generation by 30 µL of DI water.

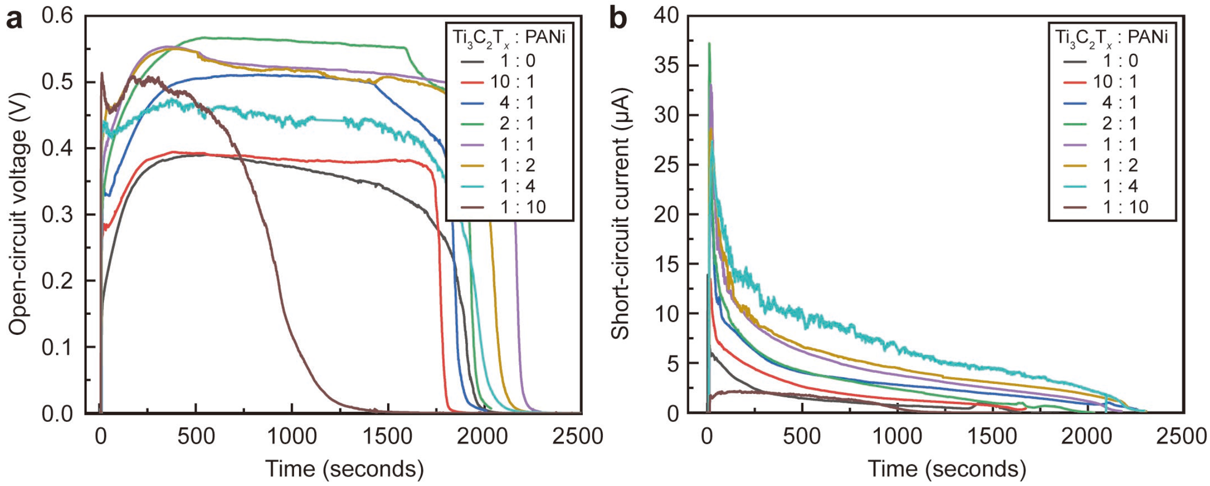

Fig. S20 Measured V_{OC} and I_{SC} from MPTEPG (250 Ω) by dropping 30 μL of DI water.

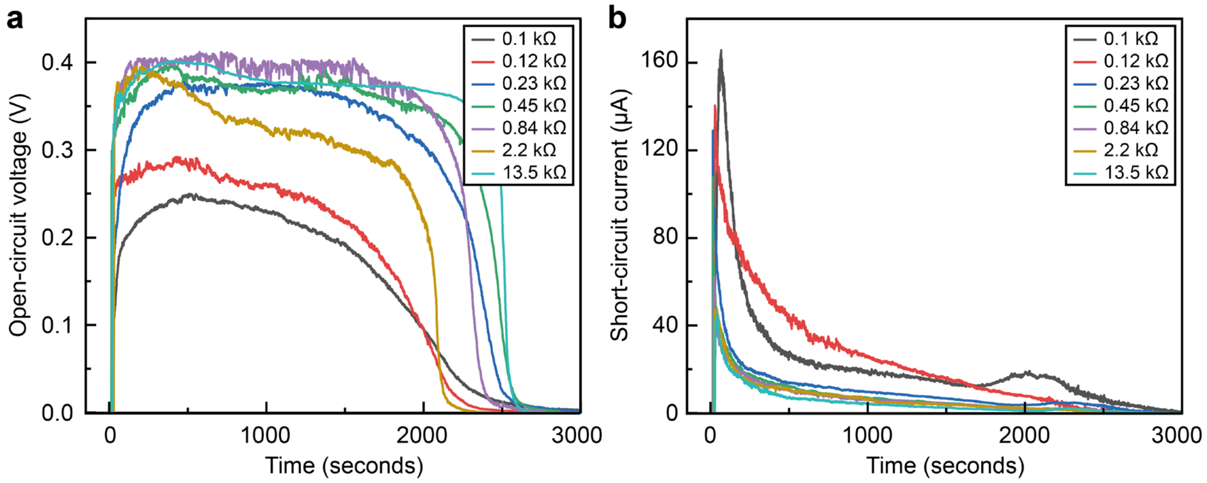

Fig. S21 Measured V_{OC} and I_{SC} of MPTEPG with varying the bulk resistance by dropping 30 μL of DI water.

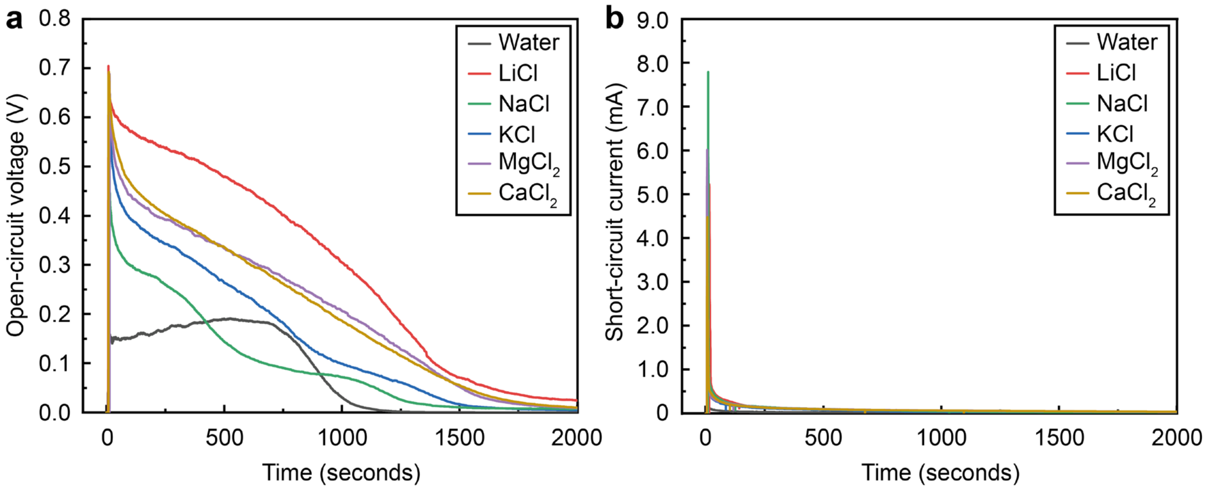

Fig. S22 Measured V_{OC} and I_{SC} of MPTEPG (250 Ω) by dropping 30 μL of 1 M of various electrolyte solutions.

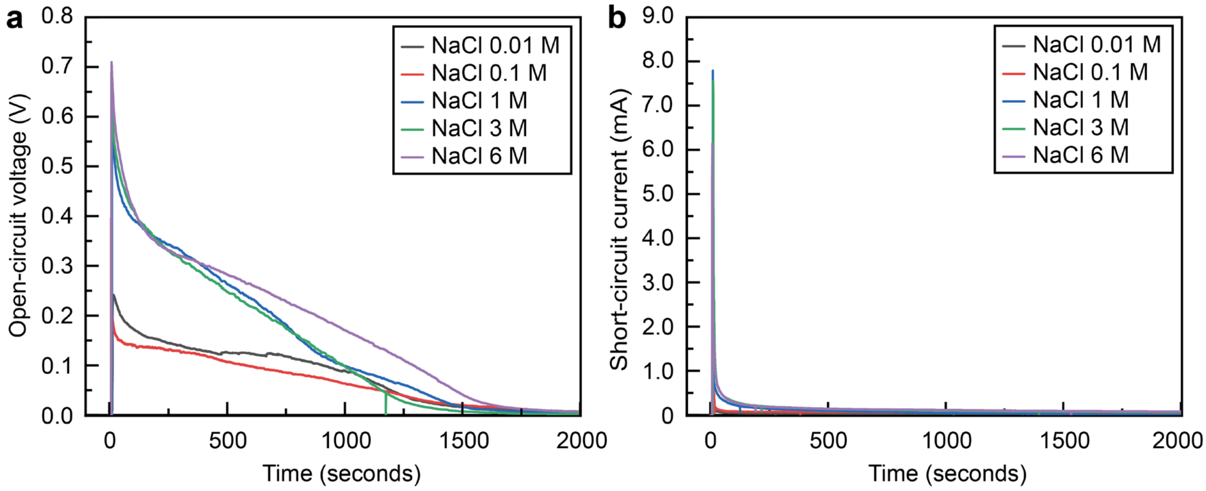

Fig. S23 Measured V_{OC} and I_{SC} of MPTEPG (250 Ω) by dropping 30 μL of NaCl solution with various concentrations.

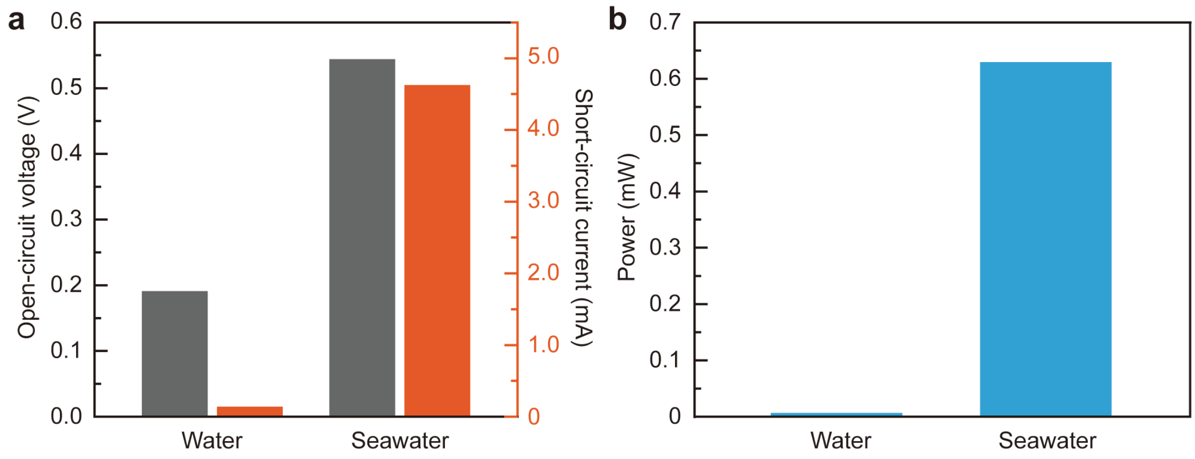

Fig. S24 Measured V_{OC} and I_{SC} of MPTEPG (250 Ω) by dropping 30 μL of water and seawater.

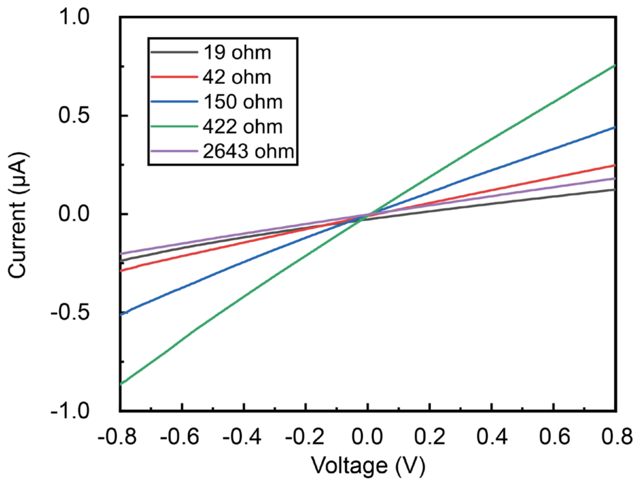

Fig. S25 I-V curves of MTEPGs with various resistances. The I-V curves were measured by applying voltage source with the scan rate of 10 mV/s at a voltage ranging from -0.85 V to 0.85 V. Based on the I-V curves, the MTEPG exhibits Ohmic contact behavior.

Table S1. The resistance of MPTEPGs with the various ratio of $Ti_3C_2T_x$: polyaniline.

Ratio of $Ti_3C_2T_x$:polyaniline	1:0	10:1	4:1	2:1	1:1	1:2	1:4	1:10
Resistance (kΩ)	1.5	1.4	1.4	1.8	1.8	2.5	3.5	76

Table S2. Summary of representative methods for hydro-electric energy harvesting. The energy performance is compared based on a single unit.

No.	**Material / Method**	**Voltage**	**Current**	**Maximum power**	**Ref.**
1	Graphene / Water stream		0.5 μA		7
2	Boron nitride nanotube / Water osmosis	0.05 V	0.0015 μA	0.019 nW	8
3	Glass and PDMS / Water stream	0.16 V	0.0018 μA	0.02 nW	9
4	MoS_2 / Water stream	0.1 V	0.01 μA	0.25 nW	10
5	MWCNT fiber / Water stream	0.18 V	24 μA	1.08 μW	11
6	Carbon / Water evaporation	1 V	0.15 μA	0.053 μW	12
7	Graphene oxide / Moisture	0.7 V	0.3 μA	0.212 μW	13
8	Reduced graphene oxide / Moisture	0.45 V	0.034 μA	0.08 μW	14
9	Graphene oxide / Water diffusion	1.5 V	0.2 μA	0.075 μW	15
10	Carbon sponge / Water evaporation	10 V (pulse)	0.02 μA	0.05 μW	16
11	Porous polydopamine / Moisture	0.52 V	1.86 μA	0.148 μW	17
12	Graphene oxide composite / Moisture	0.6 V	0.12 μA	0.007 μW	18
13	Mxene & Kevlar / Water osmosis	~0.12 V	4.8 μA	0.123 μW	19
14	Carbon nanoparticle / Water stream	0.74 V	22.5 μA	2.02 μW	20
15	Protein nanowire / Moisture	0.5 V	17 μA	1.4 μW	21
16	$Ti_3C_2T_x$ MXene / Water diffusion	0.15 V	3.6 mA	6 μW	22
17	$Ti_3C_2T_x$ MXene / Water stream	0.688V	7.55 mA	1.3 mW	This work

Table S3. Detailed analysis of XPS data from pristine MTEPG and after an operation; chemical states, peak binding energy, full width at half maximum (FWHM), and atomic percent of Ti 2p ($2p_{3/2}$, $2p_{1/2}$) and C1s.

	Component	**Peak binding energy (eV)**	**FWHM (eV)**	**Atomic (%)**
Ti 2p ($2p_{3/2}$, $2p_{1/2}$) from pristine MTEPG	Ti-C	453.90, 459.95	1.50	36.6
	Ti(II)	455.11, 461.16	1.94	40.61
	Ti(III)	456.86, 463.00	1.94	15.49
	Ti(IV)-TiO_2	458.28, 464.83	1.37	7.29
Ti 2p ($2p_{3/2}$, $2p_{1/2}$) from MTEPG after an operation	Ti-C	454.30, 460.35	1.26	36.15
	Ti(II)	455.41, 461.46	1.69	39.48
	Ti(III)	456.83, 462.88	1.70	15.36
	Ti(IV)-TiO_2	458.51, 464.56	1.48	9.01
C 1s from pristine MTEPG	C-Ti-Tx	280.97	1.05	10.25
	C-Ti-Tx	283.90	1.96	27
	C-C	284.62	1.58	44.43
	CHx/CO	286.05	2.15	12.62
	O-C=O	288.49	2.17	5.7
C 1s from MTEPG after an operation	C-Ti-Tx	281.40	0.78	12.36
	C-Ti-Tx	282.02	1.42	3.01
	C-C	284.58	1.67	73.04
	CHx/CO	286.20	1.75	7.04
	O-C=O	288.62	1.42	4.55

Table S4. Detailed analysis of XPS data from polyaniline emeraldine-base and $Ti_3C_2T_x$/polyaniline emeraldine-base; chemical states, peak binding energy, full width at half maximum (FWHM), and atomic percent of N1s.

	Component	Peak binding energy (eV)	FWHM (eV)	Atomic (%)
N 1s from polyaniline emeraldine-base	–N=	398.5	1.7	33.07
	–NH–	399.6	1.68	55.18
	N^+	401.1	1.35	10.34
		402.6	0.67	1.42
N 1s from $Ti_3C_2T_x$/polyaniline	–N=	398.5	3.06	23.41
	–NH–	399.6	1.38	39.92
	N^+	401.1	2.6	32.18
		402.65	0.97	4.5

Video S1. Operation of the blue LED (rated voltage of 3.0-3.2 V and rated current of 20 mA) powered by 24 MPTEPGs (six series connections of four parallel connections).

Video S2. Demonstration of charging a commercial lithium polymer battery (30 mAh, rated charging voltage of 5 V and current of 1 A) by 160 MPTEPGs (10 series connections of 16 parallel connections).

Supplementary References

1. Shah, S. A. *et al.* Template-free 3D titanium carbide ($Ti_3C_2T_x$) MXene particles crumpled by capillary forces. *Chem. Commun.*, 2017, **53**, 400–403.
2. Zhang, C. J. *et al.* Oxidation Stability of Colloidal Two-Dimensional Titanium Carbides (MXenes). *Chem. Mater.*,2017, **29**, 4848–4856.
3. Golczak, S., Kanciurzewska, A., Fahlman, M., Langer, K. & Langer, J. J. Comparative XPS surface study of polyaniline thin films. *Solid State Ionics*, 2008, **179**, 2234–2239.
4. Ando, R. A., do Nascimento, G. M., Landers, R. & Santos, P. S. Spectroscopic investigation of conjugated polymers derived from nitroanilines. *Spectrochim. Acta - Part A Mol. Biomol. Spectrosc.*, 2008, **69**, 319–326.
5. Zeng, X. R. & Ko, T. M. Structures and properties of chemically reduced polyanilines.

Polymer, 1998, **39**, 1187–1195.
6. Nakajima, T. *et al.* Study on the Interconversion of Unit Structures in Polyaniline by X-ray Photoelectron Spectroscopy. *Macromolecules*, 1989, **22**, 2644–2648.
7. Guo, W. *et al.* Bio-inspired two-dimensional nanofluidic generators based on a layered graphene hydrogel membrane. *Adv. Mater.*, 2013, **25**, 6064–6068.
8. Siria, A. *et al.* Giant osmotic energy conversion measured in a single transmembrane boron nitride nanotube. *Nature*, 2013, **494**, 455–458.
9. Zhang, R. *et al.* A Streaming Potential/Current-Based Microfluidic Direct Current Generator for Self-Powered Nanosystems. *Adv. Mater.*, 2015, **27**, 6482–6487.
10. Feng, J. *et al.* Single-layer MoS_2 nanopores as nanopower generators. *Nature*, 2016, **536**, 197–200.
11. Xu, Y. *et al.* A One-Dimensional Fluidic Nanogenerator with a High Power Conversion Efficiency. *Angew. Chemie - Int. Ed.*, 2017, **56**, 12940–12945.
12. Xue, G. *et al.* Water-evaporation-induced electricity with nanostructured carbon materials. *Nat. Nanotechnol.*, 2017, **12**, 317–321.
13. Liang, Y. *et al.* Electric power generation: Via asymmetric moisturizing of graphene oxide for flexible, printable and portable electronics. *Energy Environ. Sci.*, 2018, **11**, 1730–1735.
14. Cheng, H. *et al.* Spontaneous power source in ambient air of a well-directionally reduced graphene oxide bulk. *Energy Environ. Sci.*, 2018, **11**, 2839–2845.
15. Huang, Y. *et al.* Interface-mediated hygroelectric generator with an output voltage approaching 1.5 volts. *Nat. Commun.*, 2018, **9**, 4166.
16. Zhu, L., Gao, M., Peh, C. K. N., Wang, X. & Ho, G. W. Self-Contained Monolithic Carbon Sponges for Solar-Driven Interfacial Water Evaporation Distillation and Electricity Generation. *Adv. Energy Mater.*, 2018, **8**, 1–8.
17. Li, L.-H. *et al.* Moisture-driven Power Generation for Multifunctional Flexible Sensing System. *Nano Lett.*, 2019, **19**, 5544-5552.
18. Huang, Y. *et al.* All-region-applicable, continuous power supply of graphene oxide composite. *Energy Environ. Sci.*, 2019, **12**, 1848–1856.
19. Zhang, Z. *et al.* Mechanically strong MXene/Kevlar nanofiber composite membranes as high-performance nanofluidic osmotic power generators. *Nat. Commun.*, 2019, **10**, 2920.
20. Bae, J., Yun, T. G., Suh, B. L., Kim, J. & Kim, I. D. Self-operating transpiration-driven electrokinetic power generator with an artificial hydrological cycle. *Energy Environ. Sci.*, 2020, **13**, 527-534.
21. Liu, X. *et al.* Power generation from ambient humidity using protein nanowires. *Nature*, 2020, **578**, 550–554.
22. Li, Y. et al. Asymmetric Charged Conductive Porous Films for Electricity Generation from Water Droplets via Capillary Infiltrating. *ACS Appl. Mater. Interfaces,* 2021, **13**, 17902–17909.